Copyright Warning & Restrictions

The copyright law of the United States (Title 17, United States Code) governs the making of photocopies or other reproductions of copyrighted material.

Under certain conditions specified in the law, libraries and archives are authorized to furnish a photocopy or other reproduction. One of these specified conditions is that the photocopy or reproduction is not to be "used for any purpose other than private study, scholarship, or research." If a, user makes a request for, or later uses, a photocopy or reproduction for purposes in excess of "fair use" that user may be liable for copyright infringement,

This institution reserves the right to refuse to accept a copying order if, in its judgment, fulfillment of the order would involve violation of copyright law.

Please Note: The author retains the copyright while the New Jersey Institute of Technology reserves the right to distribute this thesis or dissertation

Printing note: If you do not wish to print this page, then select "Pages from: first page # to: last page #" on the print dialog screen

NJIT
New Jersey's Science & Technology University

The Van Houten library has removed some of the personal information and all signatures from the approval page and biographical sketches of theses and dissertations in order to protect the identity of NJIT graduates and faculty.

ABSTRACT

SYNTHESIS AND CHARACTERIZATION OF HAFNIUM CARBIDE THIN FILMS

by
Wiriya Thongruang

Hafnium carbide thin films of various characteristics were deposited on silicon substrates using dc magnetron sputtering. A HfC target was used as a sputtering source and Ar was used as a sputtering gas during deposition. The variables investigated were total sputtering gas pressure and power. Optimum characteristics were achieved with a total sputtering gas pressure of 5 mTorr and power of 200 W. No evidence for oxidation of the film was found at a depth below 400Å for deposited and annealed films. Binding characteristics were obtained from ESCA data. The compressive film stress increased when sputtering gas pressure decreased. The lowest HfC film resistivity achieved was 210 $\mu\Omega$-cm. This resistivity was obtained by using a low sputtering gas pressure. High power reduced film resistivities. Very low base pressures and cycling of chamber were found to lower the resistivity. Annealing of HfC deposited film reduced the stress and resistivity by approximately 10%.

SYNTHESIS AND CHARACTERIZATION OF HAFNIUM CARBIDE THIN FILMS

by
Wiriya Thongruang

A Thesis
Submitted to the Faculty of
New Jersey Institute of Technology
in Partial Fulfillment of the Requirements for the Degree of
Master of Science in Engineering Science

Interdisciplinary Program in Materials Science and Engineering

January 1997

Blank Page

APPROVAL PAGE

SYNTHESIS AND CHARACTERIZATION OF HAFNIUM CARBIDE THIN FILMS

Wiriya Thongruang

Dr. Roland A. Levy, Thesis Advisor — Date
Distinguished Professor of Physics, NJIT

Dr. Robert B. Marcus, Committee Member — Date
Research Professor of Electrical and Computer Engineering, NJIT

Dr. Trevor A. Tyson, Committee Member — Date
Assistant Professor of Physics, NJIT

BIOGRAPHICAL SKETCH

Author: Wiriya Thongruang

Degree: Master of Science in Engineering Science

Date: January 1997

Undergraduate and Graduate Education:

- Master of Science in Engineering Science,
  New Jersey Institute of Technology, Newark, NJ, 1997

- Bachelor of Science in Mechanical Engineering,
  Prince of Songkla University, Hatyai, Thailand, 1990

Major: Material Science and Engineering

This work is dedicated to
my parents

ACKNOWLEDGMENT

I would like to express my appreciation to Prof. Roland A. Levy who served as my thesis advisor, providing valuable resources and energetic advice. Special thanks are given to Prof. Robert B. Marcus, Prof. Trevor A. Tyson and Prof. S. Korenev for their reading and valuable comments. Thanks to Prof. James Grow for his value support on X-ray diffraction measurement and counseling and Dr. N. M. Ravindra for sheet resistance measurement. I thank Henry Krautter from Bell Labs-Lucent Technology for ESCA analysis, and Vitaly Sigal who gave advice for this accomplishment. I also wish to thank Dr. Roumiana Petrova and all CVD laboratory members for their helps.

TABLE OF CONTENTS

Chapter	Page
1 INTRODUCTION	1
1.1 Objective	1
1.2 Background Information	3
2 SPUTTERING THEORY AND SYSTEMS	7
2.1 Interactions of Ions with Surfaces	7
2.1.1 Ion Bombardment of a Surface	7
2.1.2 The Mechanisms of Sputtering	10
2.2 Planar Magnetron Sputtering	11
2.3 The Magnetron Cathode	17
2.3.1 Cathode Geometry and Electron/Ion Motion	18
2.3.2 Target Erosion and Film Uniformity	20
2.4 A Conventional DC Sputtering System	21
2.4.1 Choosing the Sputtering Gas	22
2.4.2 Choosing the Gas Pressure	22
2.5 Practical Aspects of Sputtering System	23
2.5.1 Ground Shields	23
2.5.2 Shutter	24
2.5.3 Target Cooling	24
2.6 Applications of Sputtering	24
2.6.1 Sputtering as a Deposited Process	25

TABLE OF CONTENTS
(Continued)

Chapter **Page**

2.7 Thin Film and Electronic Applications........ 25

3 IMPLEMENTATION........ 27

3.1 Experimental Specifications........ 27

3.2 Sputtering System........ 29

3.2.1 Equipment Setup........ 29

3.3 Sputter Deposition Procedures........ 30

3.3.1 Presputtering........ 30

3.3.2 Sputter Deposition........ 30

3.4 HfC Film Characterization Techniques........ 30

3.4.1 Physical Property........ 30

3.4.1.1 Film Thickness........ 31

3.4.2 Structural Property........ 31

3.4.2.1 X-ray Diffraction Analysis........ 31

3.4.3 Electrical Property........ 31

3.4.4 Mechanical Property........ 33

4 RESULTS AND DISCUSSION........ 35

4.1 The Effects of Variables on Deposition Rate........ 35

4.1.1 Power Dependent Study........ 35

4.1.2 Total Gas Pressure Dependent Study........ 36

TABLE OF CONTENTS
(Continued)

Chapter **Page**

4.2 HfC Film Characteristics 37

4.2.1 Physical Properties 37

4.2.1.1 X-ray Diffraction Analysis 37

4.2.1.2 Atomic Concentration Analysis 40

4.2.1.3 Binding Energy Analysis 42

4.2.2 Mechanical Property 43

4.2.2.1 Stress 43

4.2.3 Electrical Property 46

4.2.3.1 Resistivity 46

5 CONCLUSIONS 49

REFERENCES 51

LIST OF TABLES

Table **Page**

1.1 Sputtering sources ... 5

2.1 Characteristics of magnetron cathode ... 19

3.1 Experimental magnetron sputtering system specifications ... 28

3.2 Experimental silicon wafer specifications ... 29

4.1 X-ray diffraction results ... 38

4.2 Atomic concentration in HfC deposited films ... 40

4.3 Influence of sputtering power on oxygen concentration ... 41

LIST OF FIGURES

Figure		Page
2.1	Three types of collision representation	8
2.2	Interactions of ions with surfaces	10
2.3	Simple schematic of the sputtering process showing and Ar^+ ion ejecting atoms and electrons from solid target and also displacing atoms with in target	12
2.4	Schematic of circular planar magnetron target assembly	15
2.5	Target erosion pattern for a circular magnetron cathode	20
2.6	Schematic of a dc sputtering system	21
2.7	Schematic of sputtering system showing ground shields, shutter, electrode and cooling system	23
3.1	Experimental schematic of dc magnetron sputtering	27
3.2	Four-point probe system for sheet resistance measurement	32
3.3	The resistivity measurement position on the wafer	33
3.4	Optical system for stress measurement setup	34
4.1	Variation of deposition rate as a function of power	35
4.2	The effect of total gas pressure on deposition rate	36
4.3	X-ray diffraction data of HfC film on silicon substrate	39
4.4	ESCA depth profile data of HfC deposited film	42
4.5	Variation of deposited film stress as a function of total gas pressure at constant power	43
4.6	Variation of deposited film stress as a function of power at constant total gas pressure	44
4.7	Film stresses as a function of film thickness	45

LIST OF FIGURES
(Continued)

Figure **Page**

4.8 Variation of resistivity of Hf thin film as a function of total gas pressure........... 46

4.9 Variation of resistivity of HfC thin film as a function of total gas pressure at constant power.. 47

4.10 Variation of resistivity of HfC thin film as a function of power at constant total gas pressure.. 48

CHAPTER 1

INTRODUCTION

1.1 Objective

There are many materials which may potentially provide outstanding opportunities for future high temperature applications. Carbon fiber reinforced carbon (CFRC) and carbon fiber reinforced SiC (C/SiC) are an example [1]. However, owing to their instability in air at high temperatures, they need protective coatings. Silicon dioxide has been widely used as a protective coating, despite its relatively low melting point. However, silicon carbide provides a far better protection. Most recently, hafnium carbide (HfC) because of its extremely high melting point of 3887 ^{0}C, lack of volatile oxidation products [2], higher strength and good corrosion resistance [3] is an interesting candidate as a component of high temperature resistant coatings due to the refractory, thermally insulating dioxide [4]. Because of its high melting point, electrical and magnetic properties, and high hardness, hafnium carbide films find applications as high temperature resistors, head of thermal pen recorders, thin protection films for magnetic heads or as a wear resistance films on cutting tools [5]. Hafnium carbide could be considered as the most effective second-phase particles in strengthening tungsten at high temperatures. W-HfC alloy appears to be a very strong high temperature metallic material [6].

Transition metal carbide have unique properties, including excellent mechanical stability and relative low work function, which could make them well suited for use as field emission (FE) cathodes operating at ambient or elevated temperatures. Their properties make them candidates for FE applications in radiation immune microcircuitry or radio frequency (rf) vacuum microelectronics and other uses such as thermionic cathodes in high temperature themionic converters [7]. Such cathode can potentially be used where the need of very high density, small spot size electron source is required. Fundamental work and characterization of the deposited layers of hafnium carbide were studied by chemical vapor deposition (CVD). The influence of the various experimental parameters in the formation of hafnium carbide thin films by plasma enhanced CVD from bis(η-cyclopentadienyl)dimethyl hafnium as a precursor has been studied [5]. CVD of nonstoichiometric hafnium carbide was studied by computer minimization of the Gibbs free energy of the system [8] and a phase diagram of the hafnium-carbon system was presented [9,10]. In addition, a phase diagram of ordered nonstoichiometric HfC also was present by Gusev [11].

The objective of this thesis is to present experimental characteristics of the HfC deposited film on pure silicon substrate using DC magnetron sputtering. Some characteristics such as microstructure, resistivity, and stress of the deposited films are examined. In addition, atomic concentration and binding energy of the films have also been investigated. The sputtering method was used due to the possibility of using lower substrate temperatures [12]. Consequently, the growth of the film does not necessarily occur under the thermodynamically equilibrium growth condition. This tends to result

in defect structures and hence different properties of the films compared to bulk materials.

Sputtered species have kinetic energy 50-100 times higher than thermally evaporated atoms [13]. leading to higher packing density. This process is widely used for deposition in microelectronic applications. Since targets have reasonable electrical conductivity, dc sputtering was used for all single-layer and multi-layer coatings [14]. Apparently, the absence of any data on the ordering of hafnium carbide in the literature is a consequence of the difficulty in performing a study of the HfC deposited films.

1.2 Background Information

As early as 1877, sputter deposition was used to deposit thin films to coat mirrors. In the 1920s, sputtering was served as the system to deposit gold for coating of flexible fabrics and subsequent electrolytic thickening. As a vacuum technology became more sophisticated, sputtering was largely replaced by vacuum evaporation or resistance heating techniques which offered higher rates of deposition.

The interest in sputtering as a film deposition technique persisted because many materials could not be evaporated by resistance heating methods. Sputtering is an atom-by-atom process. The target is bombarded by ions of gas which physically chips atoms off the target, causing them to be ejected from the surface and subsequently strike the substrate and adhering. In this manner, a high quality film is gradually built up.

Physical sputtering is a non-thermal vaporization process in which the surface atoms are physically ejected by momentum transfer from an energetic bombardment

particle, which is usually an ion-accelerated from a plasma. Sputter deposition may be performed at low gas pressure (<5 mTorr) where the sputtered particles do not suffer gas phase collisions or in a higher gas pressure (5-30 mTorr) where energetic particles from sputtering target are thermallized by gas phase collisions before they reach the substrate surface [15].

The advantages of sputter deposition are:

- Good film adhesion is assured.
- Low temperature epitaxy is possible.
- Film thickness control is simple and easily reproduced.
- Thickness uniformity over larger planar areas can be obtained.
- The sputtering target provides a stable, long-lived vaporization source.
- Refractory materials, Multicomponent and insulating films can be deposited.

The disadvantages of sputter deposition are:

- The source material must be available in sheet form.
- The deposition rate is usually less than 2000 A^0/min.
- The substrate must be cooled unless low deposition rates or short runs are acceptable.
- In some configuration, gaseous contamination is not easily removed from the system. When they are activated in the plasma, film contamination is more of a problem than it is in vacuum evaporation.

There are also a number of sputtering systems which can be used for film deposition, as shown in Table 1.1 [16].

Table 1.1 Sputter sources

Approximate Pressure	Method
0.01 Pa	Ion Beams: duoplasmotron, ion thruster
0.05 Pa	Magnetrons: dc, rf, planar, sputter gun, cylindrical (post), orbitorr
0.50 Pa	RF: diode, magnetic enhancement, insulators, conductors
0.50 Pa	DC triode: cylindrical, separated, magnetically enhanced
1.50 Pa	DC diode: planar, cylindrical, getter, bias
1.50 PA	AC

However, they differ only in the means used to deliver ions to the sputtering source or target. Except for the ion gun systems, the target is immersed in a gas discharge; in the ion gun case, the discharge is remote from the target and ions are accelerated out of the discharge to the target [17]. Although this method bears a strong resemblance to electron beam evaporation and would be very suitable for comparison of

the two processes, it is not generally used because it does not provide high deposition rates.

Of the method listed in Table 1.1, magnetron sputtering is the most widely used. It retains many of the characteristics of the diode discharges first used by Grove and others. Magnetron sputtering generally provides higher deposition rates and lower substrate temperatures than other methods. However, its wide application in microelectronics is due to the use of electric and magnetic field geometries to prevent high energy electrons from reaching the substrate. This minimizes the generation of trapping centers in the semiconductor or device structure. Since the geometrical requirements of orthogonal electric and magnetic fields providing a closed-electron path can be met in many ways, there are many variations of magnetron systems but we will discuss only planar magnetron since this is most widely used in microelectronics.

Sputter deposition is widely used to deposit thin film metallization on semiconductor material, coating on architecture glass, reflective coatings on compact discs, magnetic films, dry film lubricants and decorative coating.

CHAPTER 2

SPUTTERING THEORY AND SYSTEMS

2.1 Interactions of Ions with Surfaces

When an ion approaches the surface of a solid usually called the *Target* one or all of the following phenomena [18] may occur: First, the ion may be reflected , probably being neutralized in the process. This reflection is known as *Ion Scattering*. Second, the impact of the ion may cause the target to eject an electron usually referred to *Secondary Electron*. Third, the ion may become buried in the target . This is *Ion Implantation*, which is used extensively in integrated circuit technology for selective doping silicon wafers and other applications such as surface treatment of steels. The ion impact may be also responsible for some structure rearrangements in the target material, or may set up a series of collisions between atoms of the target, possibly leading to the ejection of one of these atoms. This ejection process is known as *Sputtering*. Any suitably energetic atomic particle impinging against a surface can cause sputtering.

2.1.1 Ion Bombardment of a Surface

The exact mechanisms by which atoms are ejected from a surface under ion bombardment are not known [19], but we can deduce some of the details of the interactions involved. An ion is essentially the same size as an atom, so when an ion impinges against a surface, it actually collides initially with a surface atom. At energies

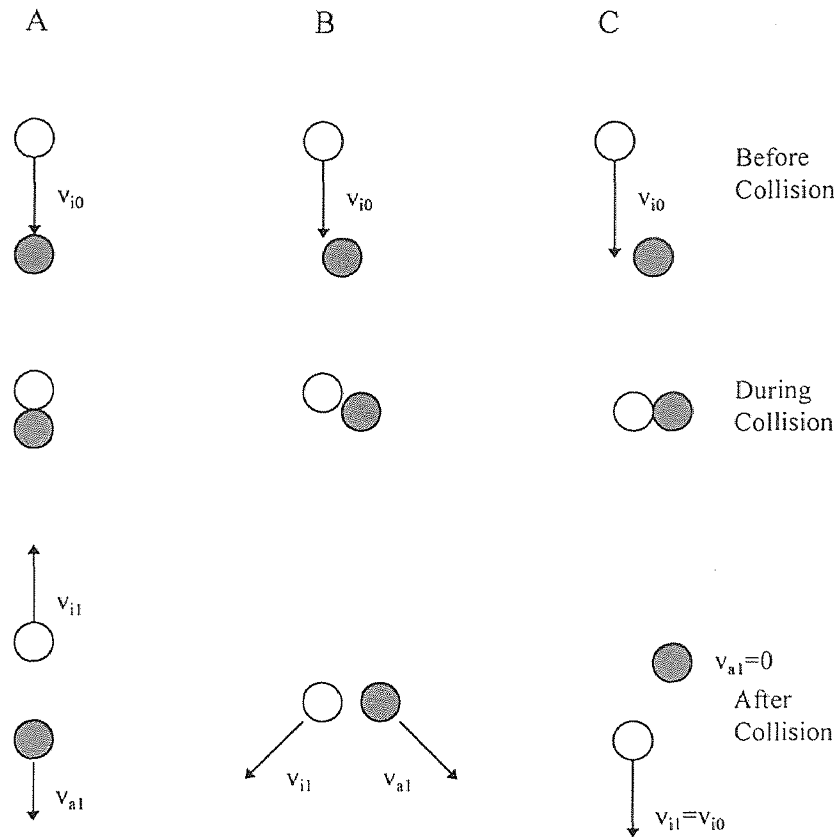

Figure 2.1 Representation of three types of collision between an incident ion and a surface atom. The mass of the incident ion is represented here being less than the mass of the struck atom. (◯ = incident ion, ● = surface atom)

at which significant sputtering occurs, the energy exchange between an incident ion and a surface atom is much grater than either lattice binding energies or vibrational energies of lattice atoms. It is most common in sputtering that the ions are incident to the bombard surface in the direction parallel to the surface normal. In this case, if the mass of incident ion is lower than the mass of the surface atom with which it collides and if the collision is head-on or nearly so, the incident ion will bounce back away from the surface (Figure 2.1A).

If the incident ion is of greater mass than the struck atom, both ion and atom will leave the point of collision in direction toward the surface interior regardless of whether the collision is head-on or glancing (Figure 2.1C). We thus have at least one and usually two particles traveling toward the interior of the surface at energies that are less than the primary energy of the incident ion or the struck atom to leave the point of secondary impact at angle greater than 45^0, so this lattice atom has a velocity component directed outward from the surface and thus has the potential of being ejected.

In the case of normal ion incidence at some energies, sputtered atoms are ejected from the surface in essentially a cosine distribution, the same as evaporated atoms. This is interesting in that the most probable direction of ejection is in exactly the opposite direction to the direction of the incident ion. Evidently the energy brought in by the incident ion is so randomly distributed by multiple collision before ejection of an atom. This result is only for the case of ion bombardment at normal incidence. In some situations, bombarding ions may be incident on the surface at oblique angles. In this case, the incident momentum vector is found to play a strong role in the ejection pattern, and the sputtered atoms are ejected very strongly in the forward direction. The sputtering yield, i.e., the number of atom ejected per incident ion, may be as much as an order of magnitude greater in the case of oblique incidence than in the case of normal incidence of the bombarding ion.

2.1.2 The Mechanisms of Sputtering

In the energy range most relevant to sputter deposition, the interaction between the impinging ion and the target atoms, and the subsequent interactions among the latter, can be treated as a series of binary collisions. The incident particle could be either an ion or a neutral atom. Ions are normally use since they can easily be accelerated by an electric field, which are neutralized by the Auger emission of an electron from the target as the ion approaches, so that the impacting species are actually mostly neutral. The series of collisions in the target [18], generated by the primary collision at the surface is known as a *Collision Cascade* (Figure 2.2).

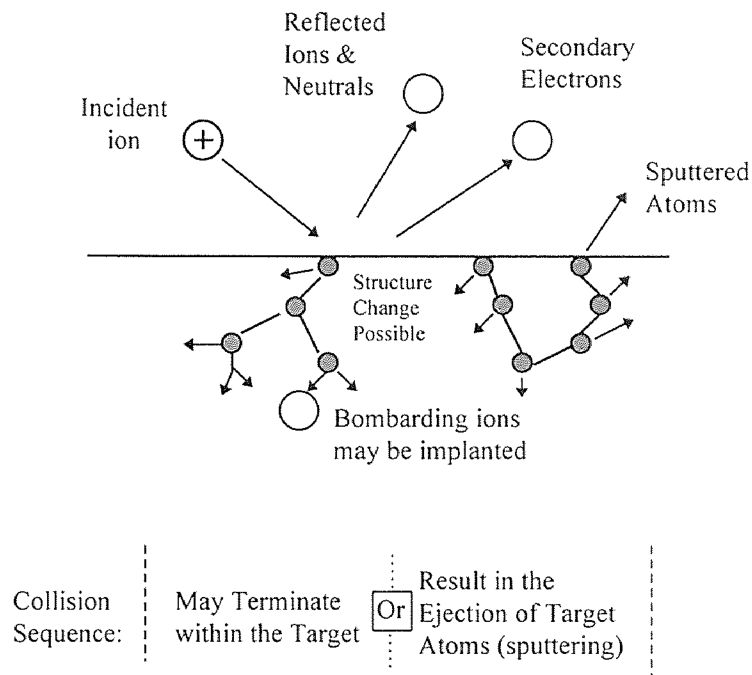

Figure 2.2 Interactions of ions with surfaces

The collision phenomena occurring in a target is often referred to *Target Kinetics*. They relate not only to sputter deposition and etching, but also to ion implantation.

2.2 Planar Magnetron Sputtering

Evaporation results from delivering energy to a solid to raise its temperature to the point where atoms obtain sufficient energy to leave the surface, sputtering is due to momentum transfer from an incident particle to atoms in the solid target [20]. To realize significant momentum transfer, the incident particle must have mass M_i comparable total target atoms M_t and the sputtering yield is given by

$$S = C \cdot \frac{4M_i M_t}{(M_i + M_t)^2} \cdot S_n(E_i) \cdot \frac{E_i}{U} \qquad (2.1)$$

where E_i is the incident particle energy, U is the surface binding energy and $S_n(E_i)$ is a function of both E_i and the particle masses. The incident particles are usually ions because they are easily accelerated to energy E_i, and the sputter yield is quoted as atoms/ion. Values of S have been collected by Anderson and Bay [21] for different combinations of M_i and M_t over a range of energies. Because of the collision sequences in the sputtering target, shown schematically (Figure 2.3), only atoms in the topmost layers of the target can gain sufficient energy to be sputtered. Because of this, sputtering using ion beams is almost universally used for depth profiling with surface analytical tools, such as electron spectroscopy.

It is evident that [16] the sputtering rate of a given target depends on the energy and number of ions bombarding the target. The sputtering rate is independent of the target temperature [21] unless the target becomes liquid. The sputter yield increases almost linearly with E_i for $E_i \leq 600$ eV so that the sputter rate is proportional to the product of J_iE_i where J_i is the ion current density.

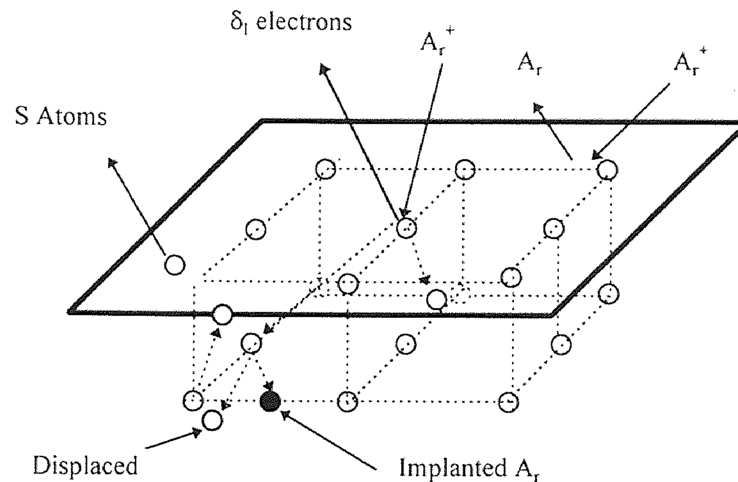

Figure 2.3 Simple schematic of the sputtering process showing an Ar^+ ion ejecting atoms and electrons from a solid target and also displacing atoms within the target while it remains in the target. An Ar^+ ion is also shown being reflected from the target surface as a neutral Ar atom [16].

From the basic grow discharge processes [18, 22-23], a secondary electron is accelerated away from the target by the negative potential V_t applied to it. As its velocity increases, it is forced to follow a circular path (Figure 2.4) due to the Lorentz forces imposed on it by the magnetic field (B) which is parallel to the target surface and thus

orthogonal to the electric field. The Lorentz force is -eVB, since the electron's orbit is in the plane orthogonal to the magnetic field, and the radius of the electron orbit is given by

$$r = \left(\frac{2m}{e}\right)^{\frac{1}{2}} \frac{V_t^{\frac{1}{2}}}{B} \tag{2.2}$$

which has a value of 3 mm for a typical magnetic field strength of 0.03T above the target surface. This field is provide by an appropriate arrangement of permanent magnets or electromagnets and provide a closed volume within which the electrons are trapped until they either lose their energy, when they are no longer subject to the Lorentz force, or cross the magnetic field lines as a result of being elastically scattered from gas atoms; the latter effect will increase with the argon pressure. During the orbit, the electron's energy increases from 0 at the target surface to 500 eV at its maximum distance from the target and begin to decrease again as it approaches the target. When it collides with an Ar atom, the latter can be ionized

$$e + Ar \rightarrow e + e + Ar^{+} \tag{2.3}$$

and both of the resultant electrons are subjected to the electric and magnetic fields. The ionization energy of Ar is 15.755 eV [24] so that a single electron could provide up to 30 Ar^{+} ions before it loses all its energy and thus escapes the magnetic trap. In fact, electrons may lose energy through other channels, such as excitation of argon atoms;

relaxation of these atoms by photon emission is mainly responsible for the bright glow discharge. The cross-section for ionization of argon by electron collisions increases rapidly from the ionization energy to approximately 50 eV. The result of the repeated electron collisions is the generation of a high density of ions and low energy electrons at a distance of a few millimeters from the target surface within the region of the magnetic trap. Because there are approximately equal number densities of electrons and ions, there is no electric field in this plasma region, which therefore has the properties of a perfect conductor. This plasma is electrically continuous with the grounded anode which is positioned within the magnetic field lines such that low energy electrons can reach it while traveling along a field line. In the plasma, up to approximately 10 % of the argon is ionized [25].

The negative potential applied to the target thus appears across the small separation between the target and the plasma; this region is called the dark space. The electric field in this region is normal to the target surface and accelerates ions from the plasma to the target; because of their much grater mass, the ions are essentially unaffected by the magnetic field.

In the planar magnetron, the ion current density at the target is very non uniform because of the shape of the magnetic trap. The highest density occurs in the region where the magnetic field is parallel to the target. The target is an equipotential surface so that an electron, emitted from the target where the magnetic field lines are almost normal to the target surface, is not trapped but is accelerated along the field line. These electrons can

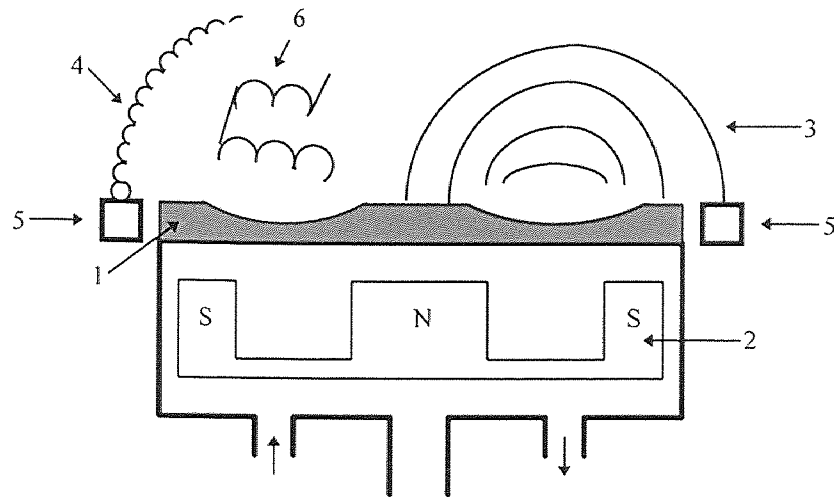

Figure 2.4 Schematic of circular planar magnetron target assembly. (1) target showing erosion track under most intense plasma (2) magnets providing (3) magnetic field lines. Low energy electrons (4) reach the anode (5) along magnetic field lines while high energy electrons cross field lines by collision with gas atoms (6).

be generated by photons from the plasma or energetic neutrons and may cause significant localized heating of the film if the field lines intersect the substrate [26]; this can be minimized by the design of the target and magnetic field. Because of the non-uniform ion current density, when the discharge impedance is low, a small voltage changes significantly affect the current and therefore the sputtering rate. Thus, a constant current or constant power supply is advisable rather than a constant voltage source. Magnetron operation at significantly lower pressure can be obtained by careful design of the magnetic field. The deposition rate for a given geometry is proportional to the sputtering rate which, as discussed earlier, should be proportional to the product $E_i \times J_i$ provided E_i

$\leq$ 600 eV. Since $E_i = V$ and J_i is proportional to I, the deposition rate, R_m, should increase linearly with the total power, IV.

The sputtering rate for each point on the target varies with J_i. The angular distribution of the sputtered atoms is given approximately by a cos θ distribution [20] as in the evaporation case. However, the degree of approximation depends on E_i, M_i and M_t. If the cos θ approximation is good and the sputtered atoms follow straight line trajectories to the substrate, the variation in deposition rate on a flat substrate parallel to a circular can be calculated since the sputtering rate actually varies significantly with the radius of the annulus, the actual deposition rates will be obtained by a weighted average for different annuli. The deposition rate varies by approximately 10% over a substrate diameter equal to the diameter of maximum erosion or about 60% of the target diameter. If the substrate is closer to the target, the uniformity becomes poorer. It should be noted that, as the target is eroded, the ejection angle, θ, is no longer normal to the original target and will vary over the eroded annulus. Thus, the deposition uniformity will change as a function of time.

The sputtered atoms will reach the substrate with both direction and the energy with which they left the target. The kinetic energy of sputtered atoms is much higher than that of evaporated atoms. Energy spectra are obtained from laser-induced fluorescence measurements. The average energy, E_{av}, per sputtered atom is obtained from the integral of the energy spectra curve [27]. Wehner and Anderson [28] showed that E_{av} generally increased with the atomic number of the sputtered atoms and with the energy of the incident ions. Thornton estimated the values of E_{av} for various metals

sputtered by Ar^+ in magnetron system. Only few of the incident ion energy is utilized in sputtering [16]; the remainder is dissipated in displacement of atoms within the target, resulting in heat. Sputtering targets must, therefore, be well cooled to prevent their temperature from rising continuously during the process. If the cooling is inadequate, the temperature may rise sufficiently for evaporation to occur.

Since the sputtered atoms pass through the plasma, they may be ionized before reaching the substrate. At high pressures, where diffusion effects are important, it has been shown [29] that ions are formed by Penning ionization and reach the substrate with very low energies unless accelerated by electric fields at the substrate [30]. The metastable energies of Ar are 11.55 and 11.72 eV [28] which are significantly above the ionization energies for some metals , so that collisions between metastable Ar and the sputtered atoms have a significant probability of forming ions. Thus, for the same sputtering power and system geometry, both the deposition rate and the uniformity will change substantially with increasing pressure. Of course, for a given pressure, diffusion effects become increasingly important as the target-substrate distance increases.

2.3 The Magnetron Cathode

Since the development of high-performance magnetron cathodes has been successful, sputtering deposition of thin films for optical and electrical applications has increased markedly. In comparison to conventional diode sputtering, the magnetron cathode provides higher deposition rates at lower operating pressures and ability to deposit high quality films at low substrate temperatures. In addition, compared with other vacuum

techniques such as evaporation, magnetron sputtered films have greater adherence and greater uniformity over large areas.

2.3.1 Cathode Geometry and Electron/Ion Motion

A Planar target consists of the target material backed by permanent magnets that provide a confinement field with the field lines forming a closed tunnel on the target surface. Secondary electrons emitted from the target during the sputtering process are accelerated across the cathode dark space towards the highly charged plasma sheath. One component of their motion is a helical line toward the center of the target. Electrons are reflected due to the higher density of field lines in this region and the repulsive electric field encountered. After reflection the electrons eventually reach the perimeter of the target where the field line again intersect the surface. An anode placed in this region effectively collects these electrons and prevents them from reaching the substrate. Another component of their motion is drift from one field line to another resulting in a race track. The combined motion give an extended path length resulting in a large number of collisions of the electrons with gas atoms. The net effect of this is an increase in plasma density close to the target, which in turn leads to higher deposition rates. Where the field lines are parallel to the cathode surface the motion of the ions is perpendicular to the target surface. Ions extracted from the plasma sheath, are accelerated across the cathode dark space and strike the target resulting in removal or sputtering of the target material. Typical operating characteristics of the magnetron cathode are given in Table 2.1 [31].

Table 2.1 Characteristics of Magnetron Cathode

Discharge parameters	
Operating pressure	0.1-10 mtorr
Direct current	
Discharge current	0.25-100 A
Discharge voltage	300-800 V
Current densities	up to 2000 A/m^2
Radio frequency	
Self-bias voltage	50-500 V
Target power	50-10 kW
Deposition rate	
High-rate metals	1-1.5 μ/min
Oxide, etc.	~0.1 μμ
Magnetic field	>0.01 T
Plasma parameters	
Electron temperature	2-20 eV
Ion temperature	0.25-2 eV
Ion/electron gyromagnetic radius	~10
Cathode dark space	~3 mm

2.3.2 Target Erosion and Film Uniformity

All magnetron targets are inherently nonuniform sources. Oscillating magnetic fields have been used to enhance sputter uniformity and target utilization [32]. The highest rate of material removal occurs where the magnetic field lines are parallel to the cathode surface. At the low pressures employed, the mean free path of the sputtered atoms is long enough that it reaches the substrate unimpeded [33]. The erosion pattern effected from operating pressure is shown schematically (Figure 2.5).

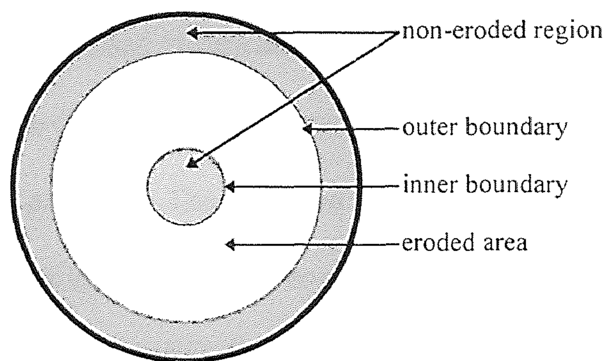

Figure 2.5 Target erosion pattern for a circular magnetron cathode

At low operating pressures, the erosion ring was broad and extended well in to the center of the target. At sufficient low pressures (< 1 mtorr), the outer boundary exceeded the target radius and the discharge was distinguished. Increase the pressure caused the boundaries to move together, thus decrease the erosion ring. These observations show that to minimize contamination of the growing film from sputtering, the guard or anode ring components at the perimeter of the target, the sputtering

parameters must be chosen carefully to maintain the erosion ring well within the target boundaries.

2.4 A Conventional DC Sputtering System

Normally in a conventional dc sputtering system (Figure 2.6) [18], the material we wish to sputter is made into a sputtering target which becomes the cathode of an electrical circuit, and has a high negative voltage V(dc) applied to it [18]. the target is nearly always solid, although powders and even liquids are sometimes used. The substrate which we wish to coat is placed on and electrically grounded anode a few inches away. These electrodes are housed in a chamber which is evacuated. Argon gas is introduced to the chamber at some specific pressure. The action of the electric field is to accelerate electron which in turn collide with argon atoms, breaking some of them up into argon ions and more electrons to produced the glow discharge.

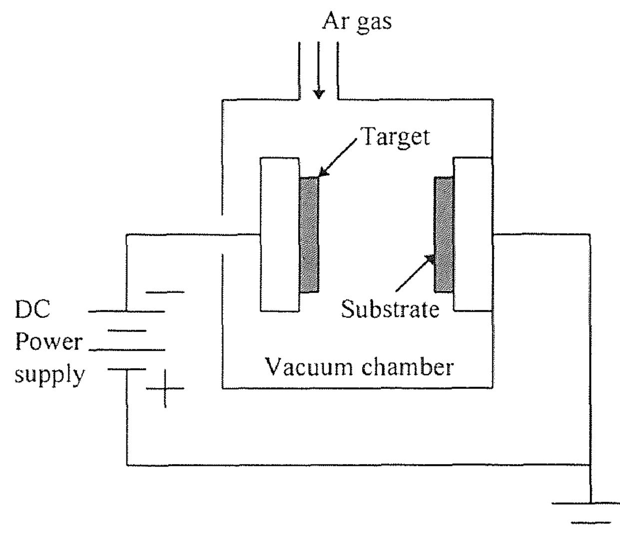

Figure 2.6 Schematic of a dc sputtering system

The charged particles produced are accelerated by the field, the electron tending towards the anode, causing more ionization on the way, and the ions towards the cathode, so that a current I flows. When the ions strike the cathode, they may sputter some of the target atoms off. They may also liberate secondary electrons from the target. The sputtered atoms from the target fly off in random directions, and some of them land on the substrate (on the anode), condense and form a thin film.

2.4.1 Choosing the Sputtering Gas

It is much easier to ionize atoms when they are in gaseous state, and easy to accelerate ions to the energies required by using and electric field which it is hard with neutrals. Noble gas ions are chosen because they do not react with the target or growing film. Sometime they are trapped by deposited film atoms but we consider this an innocuous happening. Argon [18] is almost always used in sputtering deposition because it is easily available and cheaper.

2.4.2 Choosing the Gas Pressure

A vacuum system enables one to control the operating pressure inside the sputtering system. Operating pressure limitations are imposed by the requirements of both the glow discharge and film deposition. The glow discharge sets a lower pressure limit. The discharge is sustained by electrons making ionizing collisions in the gas. The number of ionizing collisions will decrease with decreasing gas density or pressure. A different problem arises from the high density or pressure because when electrons undergo

collision, material sputtered from the target may collide with gas atoms on it way to the substrate, and will increase gas pressure. The result of the collision is to deflect the sputtered atom, and hence decrease the deposition rate.

2.5 Practical Aspects of Sputtering System

2.5.1 Ground Shield

The target is surrounded by a dark space shield, also known as a ground shield as shown below (Figure 2.7). The purpose of ground shield is to restrict ion bombardment and sputtering to the target only.

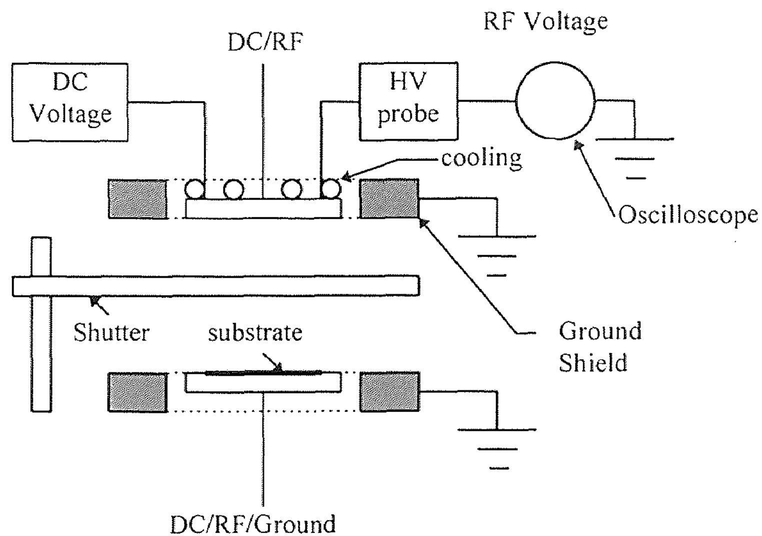

Figure 2.7 Schematic of sputtering system showing ground shields, shutter, electrode and cooling system

2.5.2 Shutter

A shutter can be rotated into place between the electrodes. This has its use during a presputtering period when the first few atomic layers of the target are removed by sputtering in order to clean it.

2.5.3 Target Cooling

Sputtering is a very inefficient process, and most of the power input to the system appears finally as target heating. Such heating can become excessive and can lead to damage of the bonding between the target and the backing electrode of the target itself.

2.6 Applications of Sputtering

The sputtering process can apply to knock an atom out of the surface of a target which is called *Sputter Etching*. By repeating this process over and over, the target surface will be cleaned or can be made thinner. In addition, it can be used to generate a topographic pattern on the surface. Besides these applications, sputter deposition can also be used. Atoms after ejected from the target under the right circumstances move through space until they strike and condenses on the surface of a receiver or substrate. By repeating the process over and over, they can build up a coating of several atomic layers of target material on the substrate. Thin film growth (refers to less than 1 μm thickness) by sputter deposition is currently the main application of sputtering.

2.6.1 Sputtering as a Deposition Process

Sputtering is a current application for the deposition of thin films. In sputtering deposition, the atom diffuse around the substrate with a motion determined by its binding energy to the substrates and is influenced by the nature as well as temperature of substrate. The atom will either jump over the barrier into an adjacent site, or might even re-evaporate. After a certain time, the atom will either evaporate from the surface or will join with another diffusing single atom to form a *Doublet*, which is less mobile but more stable than single atom.

The chance probability of forming the atomic pair will depend on the single atom density and hence on deposition rate. In time, the doublets will joined by other single atoms to form triplets and so on. This is the *Nucleation State* of thin film growth, leading to the formation of quasi-stable *Islands*. The islands grow in size rather than in number. Eventually, they grow large enough to touch, this is the *Agglomeration or Coalescence* stage which will proceeds until the film continuity. If surface atoms are mobile, they have a greater opportunity of finding low energy positions, consistent with crystal growth, in the growing film. Mobility is enhanced by increase substrate temperature. But since it also takes time to find an energetically favorable lattice position, crystal growth is also encouraged by low deposition rates.

2.7 Thin Film and Electronic Applications

Electronic applications may be more widely recognized as applications of vacuum deposited thin films. There are thin film resistors, capacitors, magnetic devices, and

active elements. But the most extensive use of vacuum deposited thin films in electronics is as electrical connection elements in integrated circuits. Basically, these electrical connection elements constitute somewhat exotic circuit boards. In some cases these may involve multi-layer coatings with conductive layers separated by nonconductive layers. There are cases where one short length of conductive element is caused to bridge over another conductive element. This is accomplished by depositing an easily etched layer between the two conductive layers and etching the intermediate coating away at the bridge point during processing.

CHAPTER 3

IMPLEMENTATION

3.1 Experimental Specifications

The sputter deposition was carried out in the TORUS^{TM}-2C Magnetically Enhanced Sputtering Cathode Assembly with its powerful Samarium-Cobalt magnets and shaped pole-pieces which enhance the magnetic field just above the plan of the target as shown (Figure 3.1). The deposition operated at the low vacuum chamber pressure. In this system 10 cm diameter silicon wafer substrates were loaded inside the chamber. The wafers were positioned under the target during deposition. Pure Argon gas (Spectra Grade) was used as deposited gas in the vacuum chamber during deposition.

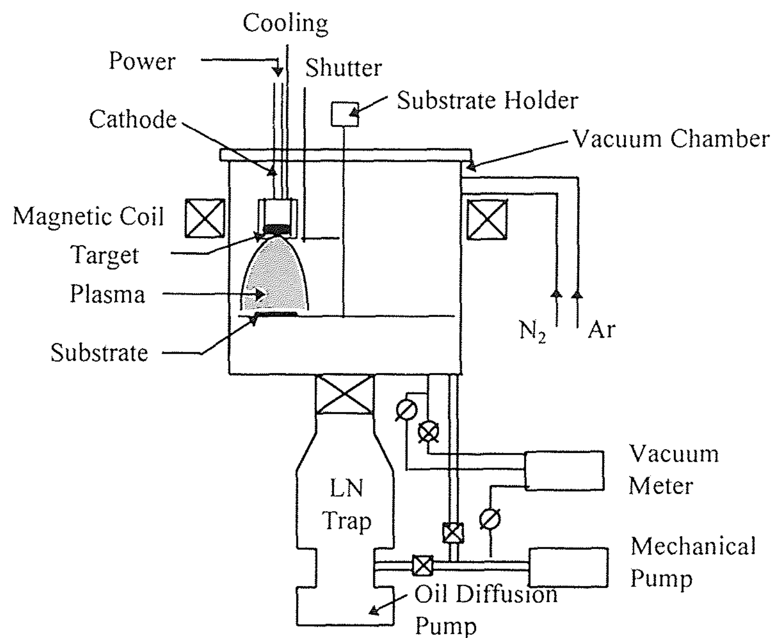

Figure 3.1 Experimental Schematic of dc magnetron sputtering

The specifications of the system are shown(Table 3.1).

Table 3.1 Experimental magnetron sputtering system specifications

Sputtering Power:	
Power Maximum (Intermittent)	1000 Watts DC
Operating Pressure	2 to 20 mTorr
Cooling Water Requirement:	
Flow rate	2 Liters/minute
Target (Deposition Material):	
Form	Plane Circular
Diameter	51 mm
Thickness	3 mm
Cooling	Indirect
Purity	99.50 %
Magnetic Enhancement	Permanent

Substrate (Silicon wafer) specifications (Table 3.2);

Table 3.2 Silicon wafer specifications which was used as experimental substrate

Diameter	100 mm
Crystal Orientation	<111>, <100>
Thickness	525±25 μm
Type	P
Resistivity	5-15 Ohm.cm
Area	77.8 cm^2

3.2 Sputtering System

3.2.1 Equipment Set up

To accomplish a sputtering run, the following steps should be taken.

1 Turn on power supply to system and turn on cooling water.

2 Open the chamber, clean and install the target in the sputtering source.

3 Position the substrates on the substrate holder.

4 Close the vacuum chamber and pump it down to a pressure 5×10^{-6} Torr or less to prevent contamination

5 Cycle the chamber 4-5 times with Ar gas and then back-fill the chamber with Ar gas to the appropriate partial pressure by using the gas-inlet needle-valve to produce the chamber pressure according to process specifications. Change an

ionization vacuum gauge for making measurement to thermo-couple gauge to prevent damage from overloading it with ions of the plasma.

6 Turn on the power supply to the sputter process.

3.3 Sputter Deposition Procedures

3.3.1 Presputtering

A sputter-shutter is used (5-10 min.) to cover the substrate during presputtering for removal of contaminants from the surface of the target. Then, the output power is slowly increased to prevent the target from breaking.

3.3.2 Sputter Deposition

Swing the shutter aside so that deposition of waiting substrate begin and swing it back when the finished deposition to prevent more sputter deposition on the substrate. Then, slowly decrease power for cooling down film on substrate to prevent oxidizing if expose the atmosphere when it is hot. Finally, stop the Ar gas flow after the power was turned off.

3.4 HfC Film Characterization Techniques

3.4.1 Physical Property

After sputter deposition, samples which are cooled to room temperature are removed for characterization.

3.4.1.1 Film Thickness: The weight change of the wafer after the deposition was measured by electro balance with 4 digits accuracy. Knowing the wafer area A (77.80 cm^2), and the mass change after deposition, Δm, HfC film thickness, t, is found from the formula

$$t = \frac{\Delta m}{\rho_b A} \tag{3.1}$$

A constant bulk density of HfC film, ρ_b, of 12.20 g/cm^3 [34] is assumed.

3.4.2 Structure Property

3.4.2.1 X-ray Diffraction Analysis: Information on the long-range structure of the HfC deposited film by sputtering was studied by X-ray diffraction measurements, using a Cu tube, on a IBM PC based Rigaku DMAX II system operating at 30 KV and 20 mA. The scanning speed of the Goniometer was 1 degree/min. HfC deposited Si wafers were scanned through a 2θ range of 20-80°.

3.4.3 Electrical Property

The resistivity can be measured by the *four-point probe* technique which is the most common methods for measuring the semiconductor resistivity. The probes are placed colinearly, as shown in (Figure 3.2). In this configuration, a constant current I is passed through two of the probes, and the voltage difference between the other two is read. For a

thin samples and non-conducting bottom wafer surface boundary, the resistivity can be calculated from the equation

$$\rho = 4.532t\frac{V}{I} \tag{3.2}$$

where t is the film thickness, V and I are voltage and current, respectively. In this experiment, sheet resistivity is measured at different locations on each wafer as shown in (Figure 3.3). The ranges of voltage and current used in measurements are 1-10 mV and <1 mA, respectively. All the measurements are taken at room temperature.

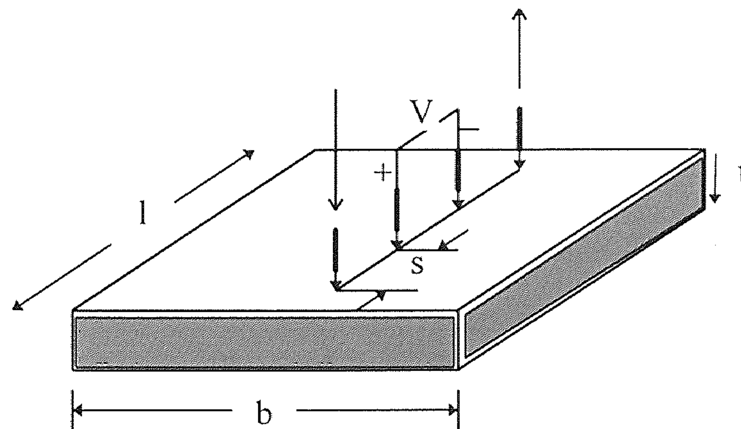

Figure 3.2 Four-point probe system for sheet resistance measurement

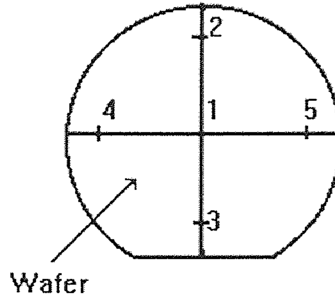

Figure 3.3 The resistivity measurement position on the wafer

3.4.4 Mechanical Property

Film stress was determined by measuring changes in the radius of curvature of a wafer resulting from deposition on a single side. The distance between two points generated by light from two fixed and paralleled He-Ne lasers was determined by reflection from the surface of a wafer before and after deposition. An angled mirror was used to project the reflection of the two points onto a wall where their separation could be accurately measured. The stress was calculated using Stoney's equation

$$\sigma_f = \frac{1}{6R}\frac{E_s d_s^2}{(1-\nu_s)d_f} \tag{3.3}$$

where E_s is Young's modulus for the substrate, ν_s is Poisson's ratio. R is the radius of curvature, d_f and d_s are the film and substrate thickness, respectively. Value of σ_f are determined through measurement of R. The film containing internal tensile stress bends the substrate concavely upward. Compressive stress developed in the film tends to initially expand the film relatively to the substrate. Internal compressive film stress,

therefore, bend the substrate convexly outward. In the present set of the fabricated laser beam equipment (Figure 3.4), the equation is reduced to

$$\sigma_f = \frac{12.3D}{d_f(\mu m)} \tag{3.4}$$

where D is the difference of the deflection of the projected laser spots after and before deposition.

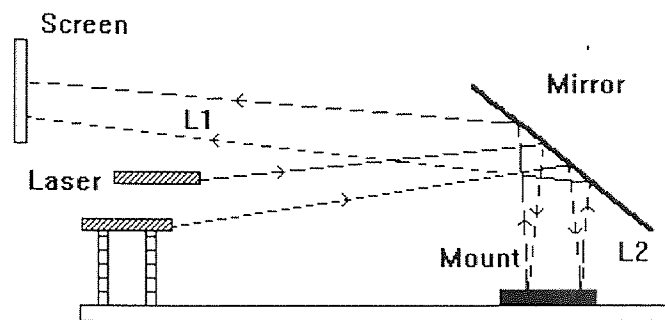

Figure 3.4 Optical system for stress measurement.

CHAPTER 4

RESULTS AND DISCUSSION

4.1 The Effects of Variables on Deposition Rate

4.1.1 Power Dependent Study

The deposition rate of HfC on Si substrate was found to increase linearly with power (Figure 4.1) under constant total gas pressure conditions. An increase in power caused a linear rise in the deposition rate because the target atoms were subjected to more intensive ion bombardment during the deposition process.

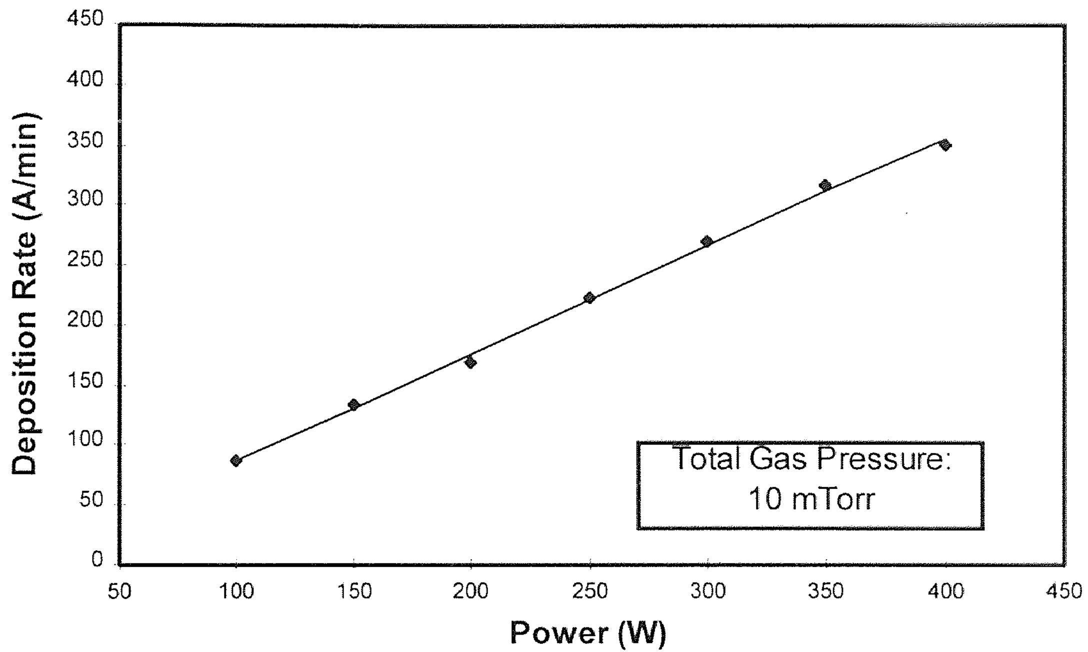

Figure 4.1 Variation of deposition rate as a function of power.

4.1.2 Total Gas Pressure Dependent Study

For constant power conditions, the deposition rate slightly decreases when total gas pressure increases from 5 to 25 mTorr (Figure 4.2). Operating pressure limitations are imposed by the requirements of both the glow discharge and film deposition. The number of ionizing collisions increase with increasing gas density or pressure. However as density or pressure increase, collisions of sputtered atoms from the target with gas atoms on their way to the substrate increase at a faster rate. The result of the collisions is to deflect the sputtered atom, and hence decreases the deposition rate.

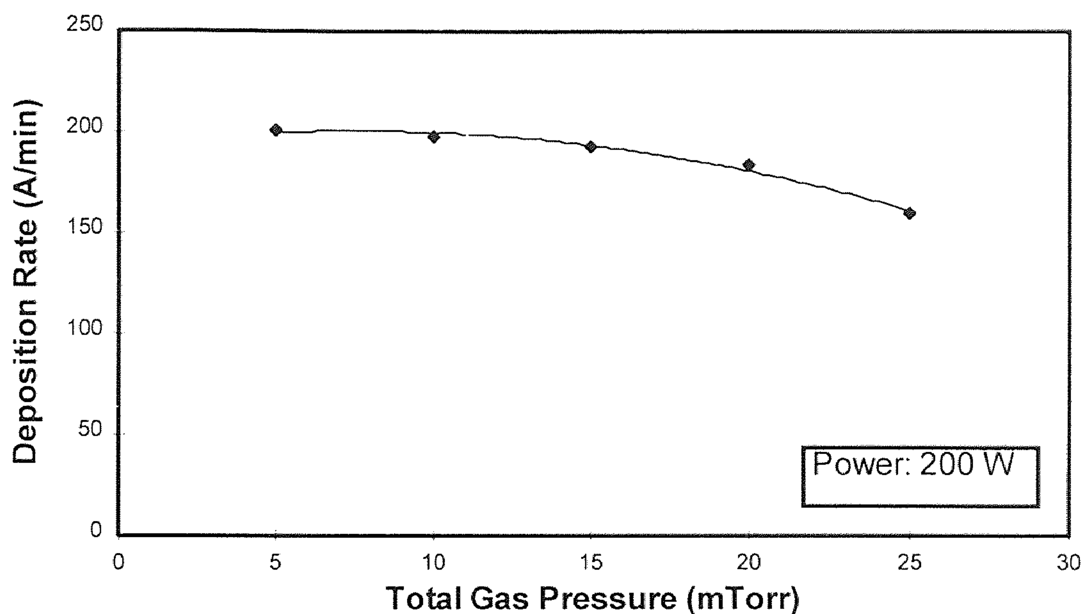

Figure 4.2 The effect of total gas pressure on deposition rate

4.2 HfC Film Characteristics

4.2.1 Physical Properties

Hafnium carbide is a transition metal carbide in which the large metal atoms of hafnium form a FCC structure with the small carbon ions present in the interstitial positions [35]. HfC has some characteristics typical of ceramics and some more typical of metals. From this experiment HfC films are metallic gray with good adhesion to the silicon substrates but some films thicker than 5000 μm had a tendency to peel off from the silicon substrates after several days which was similar to the film studied by CVD [5]. We now discuss the effects of some important sputtering variables on the properties of the deposited HfC films.

4.2.1.1 X-ray Diffraction Analysis: The types of phase and orientation of HfC film prepared by dc magnetron sputtering were examined by X-ray diffraction analysis. The total gas pressure series and power series were investigated. In table 4.1, the interplanar spacing (d) of HfC samples in different orientations (hkl) are compared to interplanar spacing of HfC solid solution. The relative intensities of the film diffraction peaks are shown.

X-ray diffraction of the sample film showed the 5 strong peaks (Figure 4.3) at 2θ of 33.52, 38.88, 55.88, 66.46 and 69.90 degree corresponding to the (111), (200), (220) and (311) planes of HfC, and (111) plane of silicon, respectively. The strongest peak is at 33.52 with d-space of 2.6713 A^0 corresponding to (111) plane of HfC. The diffraction profile is consistent with that of solid HfC.

Table 4.1 X-ray diffraction data show interplanar spacing d and relative intensity of sample (200 watts, 5 mTorr) comparing to the data from solid solution.

Plane (hkl)	Interplanar Spacing d (A^0)		Relative Intensity I(REL)
	Solid Solution	Experiment	
(111)	2.680	2.6713	100
(200)	2.321	2.3145	30.19
(220)	1.641	1.6440	18.77

The d-space in (111) orientation was lower than of solid solution but in the (200) and (220) orientations were higher. An increase in d-space might be due to excess carbon which would expand the lattice constants. The decrease in d-space of the film has been discussed previously. Liu and Cowley [6] showed that the d-spacing of HfC decreases with excess-hafnium or hafnium-rich HfC. Kieffer and Ettmayer [35] indicated that the presence of oxygen also reduces the lattice spacing or d-spacing similar to the reduction caused by carbon vacancies. The crystal structure of HfC has been determined by Cotter and Kohn [37]. It was found that HfC has a NaCl structure with a lattice parameter a_0 equal to 4.641 Å.

X-ray data revealed the influence of the total gas pressure on the peak intensity of the HfC films. The highest peak intensity could be found when the total gas pressure was in the range of 5-10 mTorr. The peak decreased when total gas pressure was raised from

10 to 20 mTorr, and the diffraction peak also was broaden similar to the study of Li-Jian Meng [38]. The film structure of this pressure range was crystalline. However, when the pressure increase from 20 to 30 mTorr, there was no crystalline phase shown. The structure changes from crystalline to amorphous when oxygen was substituted into HfC films. By varying of power or thickness, the X-ray data did not reveal much differences in the relative intensity of the HfC deposited film.

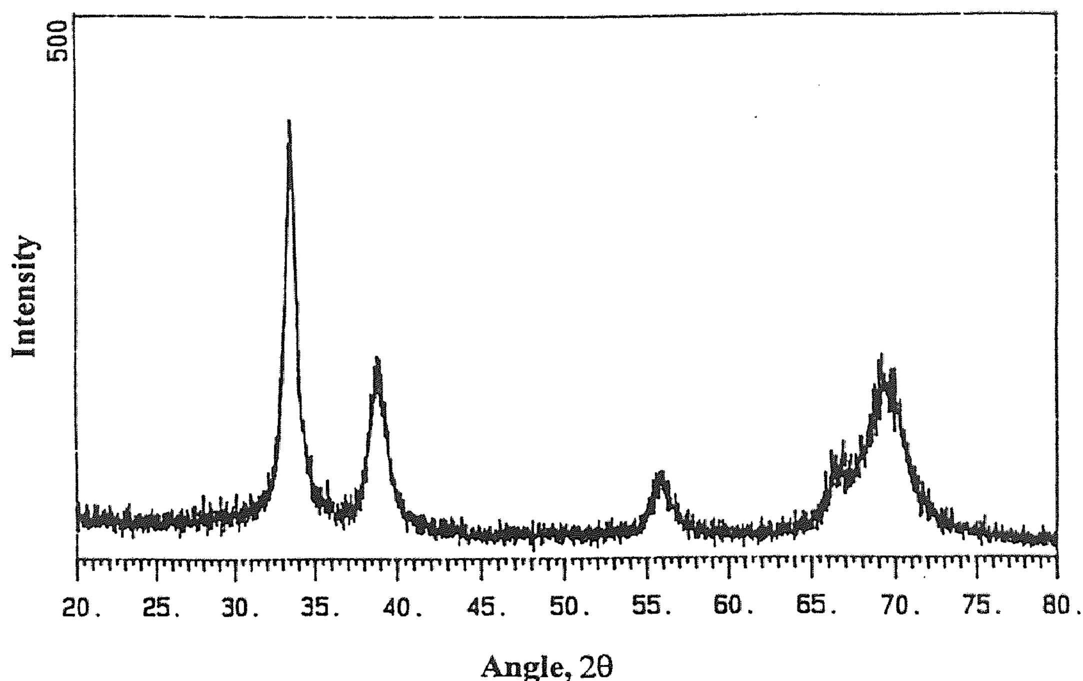

Figure 4.3 X-ray diffraction data of HfC film on silicon substrate.

After annealing at a temperature of 600 ^{0}C for 30 minute in 1 Torr vacuum pressure, the peak height increased which implied an increase in Hf-C intensities. However, the film oxidized when annealed at higher temperature.

4.2.1.2 Atomic Concentration Analysis: The atomic composition and the impurity content in the HfC thin film can be determined from Electron Spectroscopy for Chemical Analysis (ESCA). In order to convert the measured peak height ratios to composition, the relative sensitivity factor of reference samples has to be known [12].

The atomic concentration in the HfC films were investigated by Bell-Labs Lucent Technology as shown in Table 4.2. The oxygen concentration increased when the total

Table 4.2 Atomic concentration in HfC deposited films as a function of total gas pressure

Total Gas Pressure (mTorr)	Atomic Concentration (%)		
	Hf_{4f}	C_{1s}	O_{1s}
5	56.03	30.88	13.09
10	47.75	20.72	31.53
20	43.61	16.76	39.63

gas pressure was increased. In contrast, the concentration of Hf and C atoms decreased when the total gas pressure was increased.

The oxygen concentration in the film was influenced by the sputtering power. The oxygen concentration in Hf and HfC deposited films decreased when the sputtering

power increased as shown in Table 4.3. However, higher sputtering power caused the ceramic-metal HfC target to break more easily than at lower power.

Table 4.3 The influence of sputtering power on oxygen concentration in Hf deposited films (200 watts, 10 mTorr)

Sputtering Power (watts)	Oxygen Concentration (%)
150	45
200	24
250	33
300	19

ESCA analyzed data revealed the variation of intensity at different depth. Below the surface, higher intensities of hafnium and carbon but lower intensities of oxygen was found. Since the atomic concentration of hafnium and carbon is very low near the surface, the bonding of hafnium and carbon atom near the film surface is also low. After annealing at 700 ^{0}C, the peaks of O_{1s} was found to increase above the value found at 600 ^{0}C. The highest intensity of hafnium and carbon could be found at annealing temperature of 600 ^{0}C. There was no oxygen (O_{1s}) in the films below 400Å from the surface of both

600^0 and 700 ^{0}C anneal. The highest concentration of 63.28% Hf_{4f} with C_{1s} of 36.72% and 0% O_{1s} could be achieved

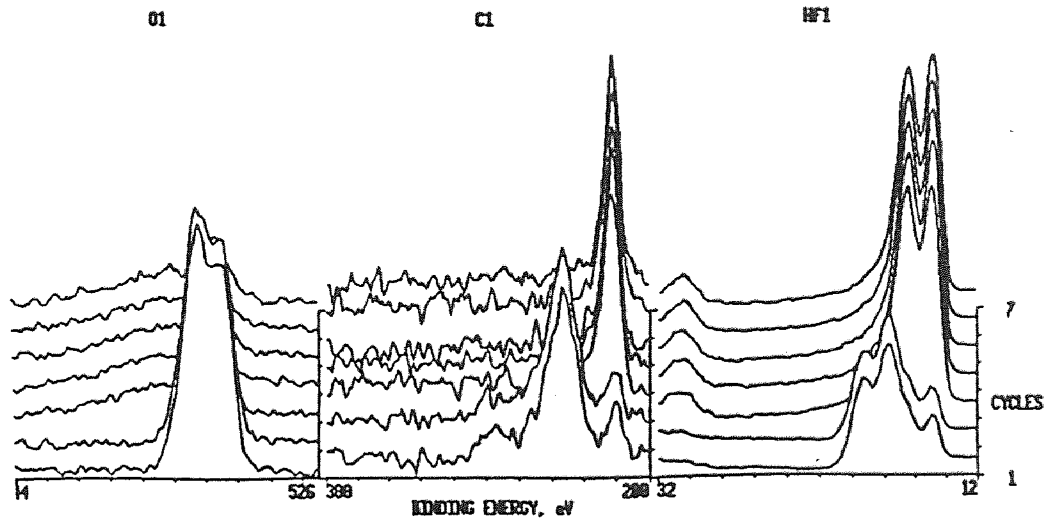

Figure 4.4 ESCA depth profile data of HfC deposited film.

4.2.1.3 Binding Energy Analysis: More details of the films in binding energy were done after 350 Å sputter etching of the 5 mTorr deposited films (Figure 4.4). The C_{1s} signal indicated the bonding energy at 286.6 eV of hydrocarbon or atomic carbon, and at 282.3 eV of the carbide bond. The Hf_{4f} was observed at 14.8 eV indicated the hafnium carbide as well as the atomic form, and 16.4 eV indicated hafnium oxide. The O_{1s} was observed at 532.3 eV represented oxide bond or atomic oxide. The binding energy of Hf_{4f}, C_{1s} and O_{1s} by CVD were studied previously [5].

4.2.2 Mechanical Property

4.2.1.1 Stress: By using a measurement of the wafer bending caused by film stress, the stress of the deposited films were determined. All observed film stresses in the total gas pressure range of 5-25 mTorr and power range of 100-400 watts were compressive. The stress rapidly decreased from 4964 MPa to 837 MPa when the total gas pressure increased from 5 to 10 mtorr (Figure 4.5). At the same total gas pressure, stress linearly increases when the power increases (Figure 4.6).

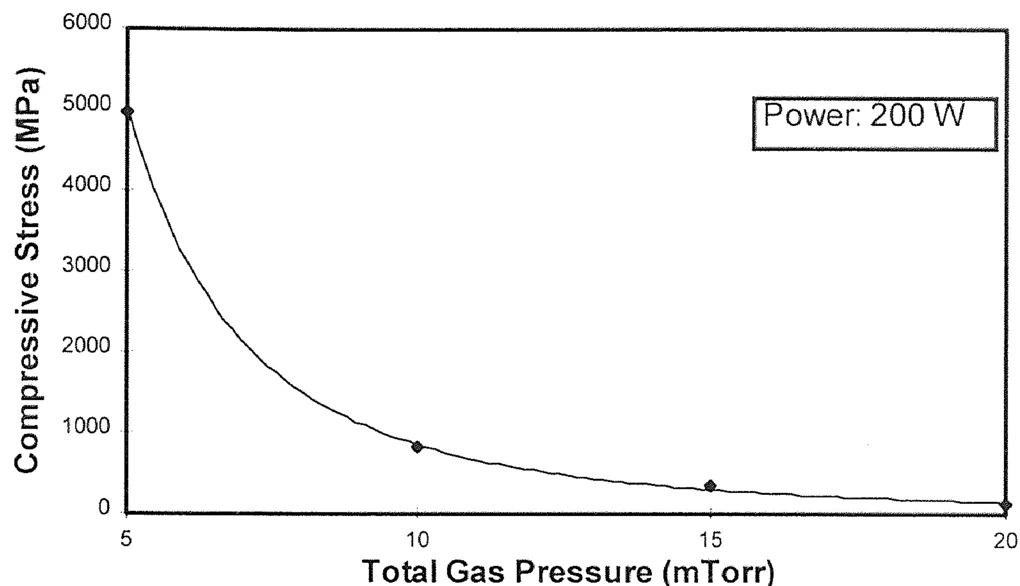

Figure 4.5 Variation of deposited film compressive stress as a function of total gas pressure at a constant power.

Most of the stress in the thin film exist because the film is bonded to a massive substrate. Thus, a change in the lattice constant along the film plane, which is not

matched exactly by an equal change in length in the substrates, will result in a stress in the film.

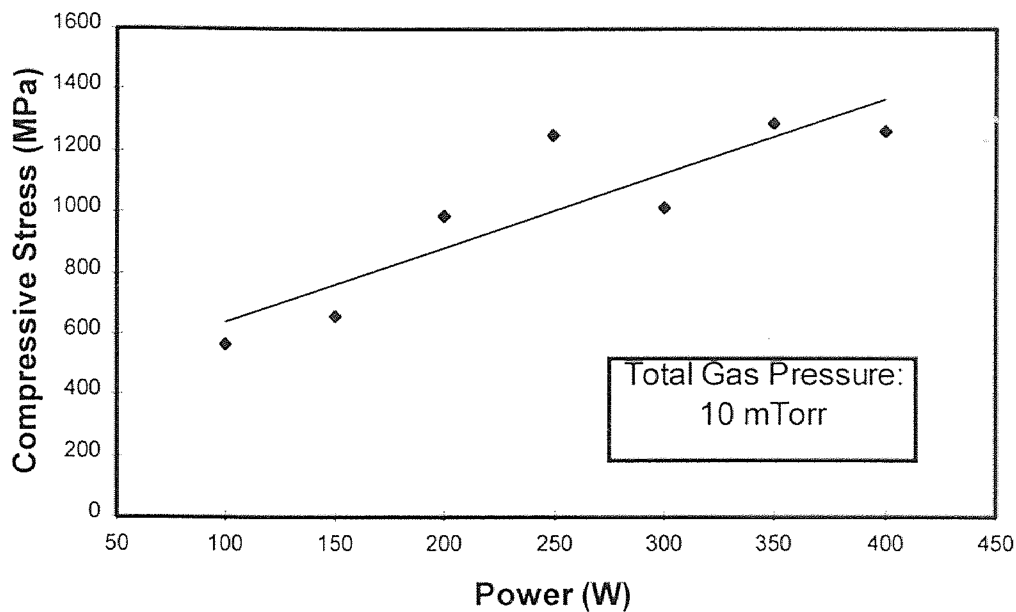

Figure 4.6 Variation of deposited film compressive stresses as a function of power at a constant total gas pressure

The most important sources of stress generation in the deposited film are incorporation of carbon, argon, oxygen and high defect concentrations. From this experiment (Figure 4.7), it is evidenced that at constant power and total gas pressure, stress is nearly constant over the deposited film thickness range of 2000-9000 A^0.

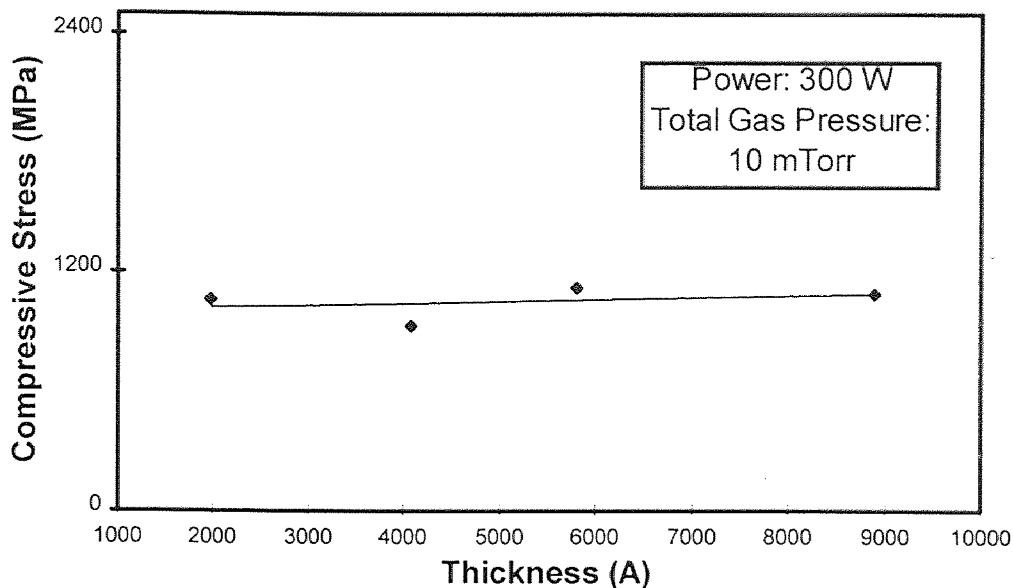

Figure 4.7 Film stresses as a function of film thickness

If sufficient oxygen is incorporated as an interstitial impurity, or if an oxide is formed having a volume larger than that originally occupied by its metal content, then the accompanying increase in specific volume should induce the intrinsic stress to become compressive. Intrinsic tensile stresses are produced by the presence of porosity or vacancies in the films.

Stress in the deposited film of HfC was decreased by about 10% after annealing samples at 600 ^{0}C and was decreased even more when annealing at higher temperatures. However, the film also oxidized at higher temperature.

4.2.3 Electrical Property

4.2.3.1 Resistivity: A resistivity value of 134±10 μΩ-cm at the surface of the film was obtained for a pure hafnium thin film. This is compared to the bulk value of 35 μΩ-cm [39]. Resistivity of pure Hf thin films increased with increasing total gas pressure (Figure 4.8). The increase of Hf film resistivity correlated with the 7-60% increase in oxygen content when the total gas pressure increased from 5 to 20 mTorr.

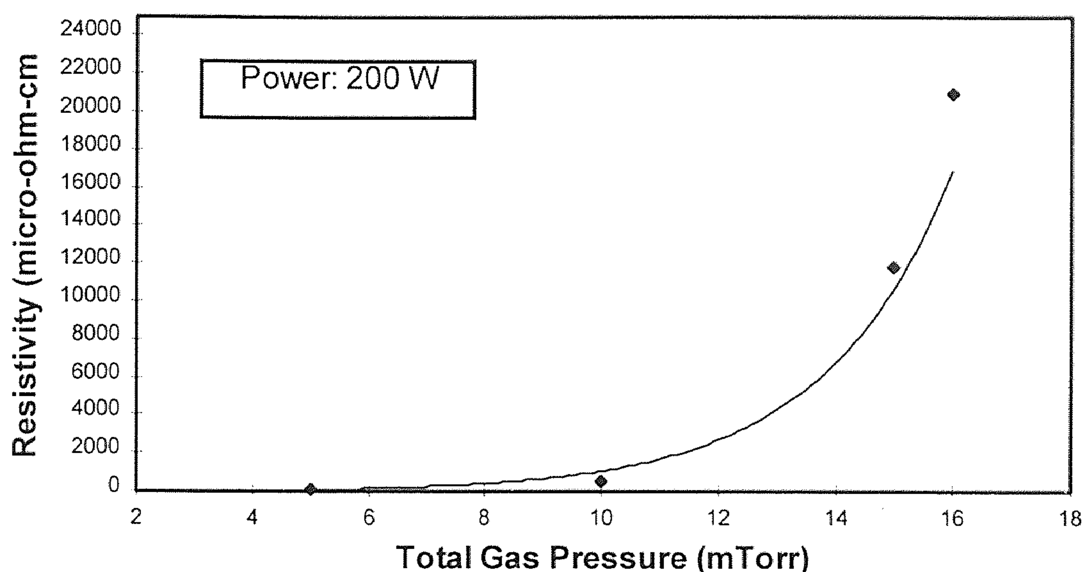

Figure 4.8 Variation of resistivity of Hf thin film as a function of total gas pressure.

From the ESCA depth profile data, the concentration of Hf-Hf and Hf-C was very low near the surface of the film and increased with depth, while the concentration of Hf-O was highest at the surface. This could result in higher resistivity near the surface. The hafnium oxide film is highly insulating corresponding to the study which was done before [4].

By sputtering, the lowest HfC film obtained was 250±40 μΩ-cm, compared with 271 μΩ-cm by CVD [5], and the 109 μΩ-cm of solid solution [34]. As the total gas pressure increases a very rapid increase in the resistivity occurs (Figure 4.9).

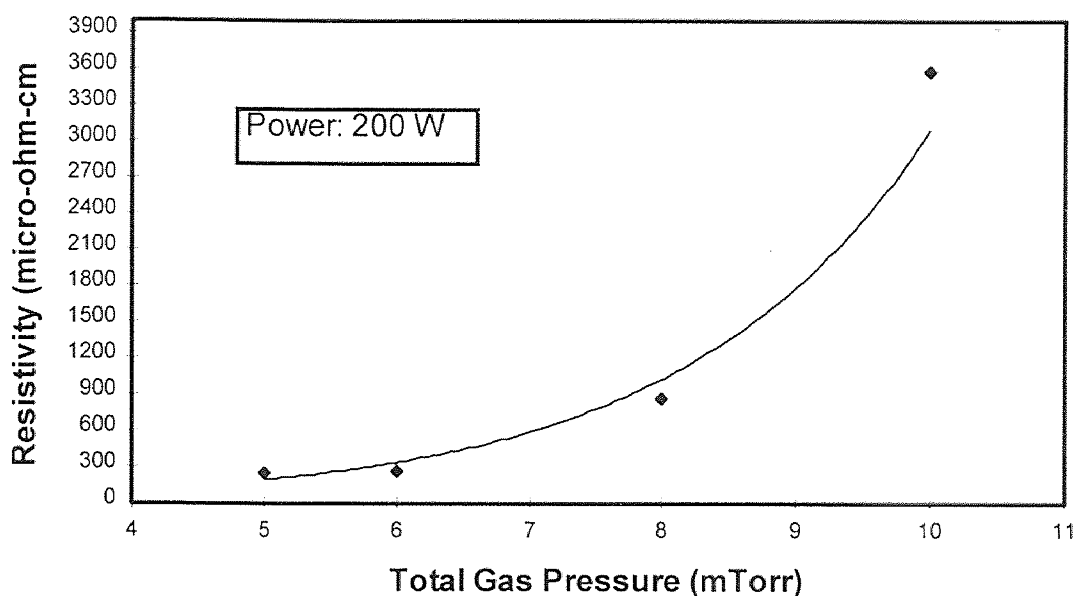

Figure 4.9 Variation of resistivity of HfC thin film as a function of total gas pressure at constant power.

It is believed that atomic oxygen can substitute for the carbon present in the interstitial sites, forming hafnium oxycarbide [3]. When the total gas pressure increased from 5 to 20 mTorr, the hafnium concentration decreased from 56.03 % to 43.61 % and carbon decreased from 30.88 % to 16.76 %. But the oxygen content increased from 13.09 % to 36.63 %. The increase in the resistivity of HfC film above the bulk material is due to impurity contents such as oxygen and also argon atoms.

The resistivity of HfC films was found to decrease when the power increased (Figure 4.10). This trend seemed to be true although at different film thickness. Base pressure before feeding argon into chamber could influence the resistivity. The resistivity decreased by more than 10% when the base pressure decreases from 2×10^{-5} to 6×10^{-6} Torr because water inside sputtering chamber was removed.

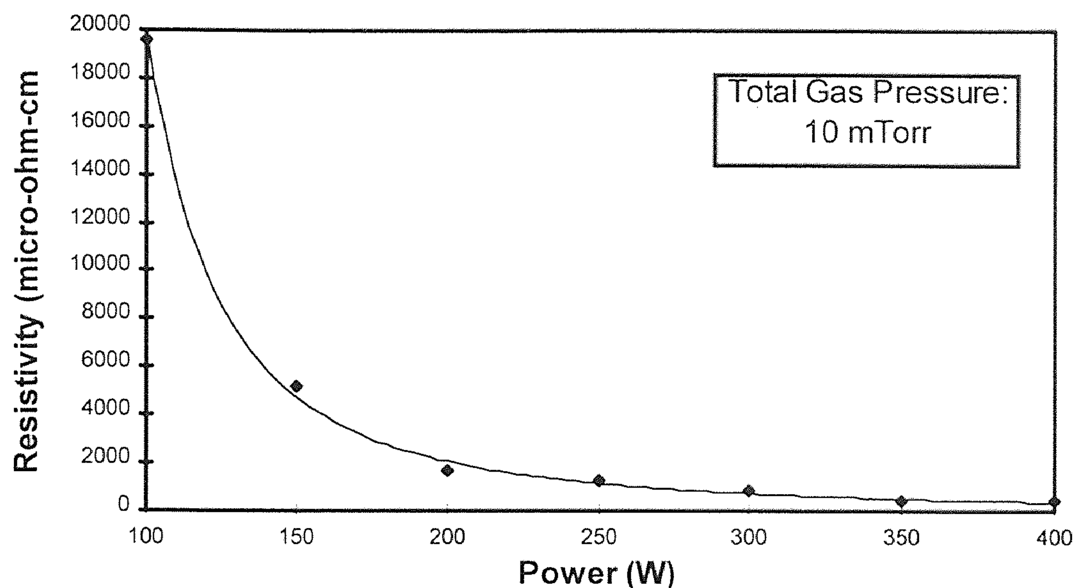

Figure 4.10 Variation of resistivity of HfC thin film as a function of power at constant total gas pressure.

The resistivity of HfC films decreased by approximately 10% after annealing at 600 ^{0}C. However, the resistivity increased slightly after annealing at 700 ^{0}C, and continued to increase on annealing at higher temperature.

CHAPTER 5

CONCLUSIONS

The purpose of this thesis was to examine characteristics of HfC films deposited using DC magnetron sputtering technology. Pure Hf films have been deposited for comparison.

Low stress of 4964 MPa and low resistivity of 210 $\mu\Omega$-cm of HfC films have successfully synthesized on pure silicon wafers in a vacuum chamber with no substrate cooling of the DC magnetron sputtering system. Ar was used as the sputtering gas. The total gas pressure range of 1-25 mTorr, power range of 100-400 watts, and deposited film thickness of 1300-8900 Å were studied. The deposition rate increased linearly with power, and increased when total gas pressure decreased. The highest deposition rate of 200 Å/min. was achieved at 5 mTorr total gas pressure. The films oxidized when deposited at higher pressure.

The X-ray diffraction patterns indicate the crystalline nature of HfC deposited films. The (111) plane showed the highest peak intensity of HfC deposited films. After anneal at the temperature of 600 ^{0}C for 30 minute in vacuum at a pressure of 1 Torr, the peak height was slightly increased.

The atomic concentration and binding energy were obtained by ESCA. The highest concentration of 63.28% Hf_{4f} was found at 400 Å from the film surface. The concentration of Hf and C decreased as the total gas pressure increased. In contrast, oxygen concentration in the films increase with increasing total gas pressure. It was seen

that the C_{1s} signal indicated the carbide bonding energy at 282.3 eV and the Hf_{4f} indicated the hafnium carbide at 14.8 eV and at 16.4 eV of hafnium oxide.

Stress of the deposited films strongly dependent on total gas pressure and power. In the pressure range of 5-25 mTorr at constant power and the power range of 100-400 watts at 10 mTorr pressure, all observed film stresses were compressive. The deposited film stress decreased as the total gas pressure increased and when power decreased. At power of 200 watts and pressure of 5 mTorr, the observed compressive film stress was 4964 MPa. The 133 MPa observed film stress could be found at 20 mTorr total gas pressure. Film stress was slightly decreased after annealing.

The lowest resistivity of 210 μΩ-cm of HfC and 134 μΩ-cm of pure Hf films were achieved at 5 mTorr and 200 watts deposition. Both Hf and HfC deposited film resistivities preferred to increase when the total gas pressure increased and increased markedly when the pressures higher than 10 mTorr. The resistivity of the HfC films decreased when the power increased. The thickness of the deposited films had no effect on resistivity. The resistivity increased with increasing oxygen. Film resistivity was slightly decreased after annealing.

REFERENCES

1. E. Fitzer, *Proc. Natl. Semin. on Recent Trends in Polymers and Composites,* Oxford & IBH Publishing Co. PVT Ltd, New York, pp. 371-388, 1987.

2. H. F. Ache, J. Goschnick, M. Sommer, G. Emig, G. Schoch and O. Wormer, "Chemical Vapour deposition of hafnium carbide and characterization of the deposited layers by secondary-neutral mass spectrometry," *Thin Solid Films,* vol 241, pp. 356-360, 1993.

3. Shiro Shimada, Michio Inagaki and Kunihito Matsui. "Oxidation Kinetics of Hafnium Carbide in the Temperature Range of 480 to 600 ^{0}C," *J. Am. Ceram. Soc*, vol. 75[10], pp. 2671-78, 1992.

4. B. C. Bargeron, R. C. Benson, N. A. Jette, T.E. Phillips, "Oxidation of hafnium carbide in the temperature range 1400 ^{0} to 2060 ^{0}C,"*J. Am. Ceramic. Soc.,* vol. 76, pp. 1040-1046, 1993.

5. P. Spatenka, H. Suhr, G. Erker and M. Rump, "Formation of hafnium carbide thin films by plasma enhanced chemical vapor deposition from bis(η-cyclopentadienyl)dimethylhafnium as precursor," *Appi. Phys.*, vol. 60, pp. 285-288, August 1995.

6. Mingqui Liu and John Cowley, "Hafnium carbide growth behavior and its relationship to the dispersion hardening in tungsten at high temperature," *Materials Science and Engineering,* vol. 60 pp. 159-167, 1993.

7. W. A. Mackie, J. L. Morrissey, C. H. Hinrichs, and P. R. Davis, "Field emission from hafnium carbide," *J. Vac. Scl. Technol.,* vol. 10(4), pp. 2852-56. 1992.

8. W. J. Lackey, J. A. Hanigofsky, and G. B. Freeman, "Experiment whisker growth and thermodynamic study of the hafnium-carbon system for chemical vapor deposition applications," *J. Am. Ceramic. Soc.,* vol. 73(6), pp. 1593-98, 1990.

9. R. V. Sara, "The hafnium-carbon system," *Trans. Metall. Soc. AIAM*, vol. 233, pp. 1683-91, 1965.

10. P. J. Spencer, K. von Goldback, R. Marazza, K. Girgis, and Kubaschewski, "Hafnium: Physici-chemical properties of its compounds and alloys," *Atomic Energy Review*, Issue no. 8, 1981.

11. A. I. Gusev, "Phase diagrams of ordered nonstoichiometric hafnium carbide and titanium nitride," *Russian Academy of Science*, vol. 322, pp. 918-923, 1992.

12. B. O. Johansson, U. Helmersson, M. K. Hibbs, and J. E. Sundgren, "Reactively magnetron sputtered Hf-N films I Composition and structure," *J. Appl. Phys.,* vol. 58(8), pp. 3104-3111, Oct. 1985.

13. G. K. Wehner and G. S. Anderson, *The nature of physical sputtering*, L. Maissel and R. Glang, Eds., McGraw-Hill, New York, Chap. 3, pp. 9-15, 1970.

14. Samad M. Edlou, Ali Smajkiewicz and Ghanim A. Al-Jumaily, "Optical properties and environmental stability of oxide coatings deposited by reactive sputtering," *Applied Optics*, vol. 32(28), pp.5601-05, Oct. 1993.

15. Leon I. Maissel and Reinhard Glang, *Handbook of Thin Film Technology*, McGraw-Hill, New York, Chap. 3-7,1970.

16. R. A. Levy, *Microelectronic Material Processes,* Kluwer Academic Publishers, Ottawa, Canada, pp. 133-201, 1989.

17. J. M. E. Harper, *Thin Film Processes*, J. L. Vossen and W. Kern, Eds., Academic Press, New York, Chapt. II, 1978.

18. B. Chapman, *Glow Discharge Processes: Sputtering and Plasma Etching,* John Wiley & Sons, New York, 1980.

19. R. V. Stuart, *Vacuum Technology, Thin Films, and Sputtering*, Academic Press, New York, 1983.

20. G. K. Wehner and G. S. Anderson, *Handbook of Thin Film Technology,* L. I. Maissel and R. Glang, Eds., McGraw-Hill, New York, p. 77, 1981.

21. H. H. Anderson and H. L. Bay, *Sputtering by Particle Bombardment* I, R. Behrisch, Ed., Springer-Verlag, Berlin, Chapt. 4, 1981.

22. J. L. Vossen and J. J. Cuomo, *Thin Film Processes,* J. L. Vossen and W. Kern, Eds., Academic Press, New York, Chapt. II, 1978.

23. W. D. Westwood, *Prog. Surf. Sci.,* vol. 7, 1976.

24. *Handbook of Chem. & Phys.*, CRC Press, West Palm Beach, Florida, pp. E-68, 59th Edition, 1979.

25. S. Schiller, V. Heisig, and K. Goedicke, *J. Vac. Sci. & Technol.*, vol. 14, pp. 815, 1977.

26. W. Class and R. Hieronymi, *Solid state Technol*, vol. 25(12), p. 55, 1982.

27. E. Dullni, *Nucl. Instrum. & Methods,* vol. B2, p. 23, 1978

28. J. A. Thronton and A. S. Penfold, *Thin Film Processes,* J. L. Vossen and W. Kern, Eds., Academic Press, New York, Chapt. II, 1978.

29. J. W. Coburn and E. Kay, *Appl. Phys. Lett.,* vol. 18, p. 435, 1971.

30. J. W. Coburn and E. Kay, *J. Appli. Phys.,* vol. 43, p. 4965, 1972.

31. K. J. Klabunde, *Thin Films from Free Atoms and Particles*, Academic Press, new York, 1985.

32. R. K. Waits, *Thin Film Processes*, J. L. Vossen and W. Kern, Eds., Academic Press, chapt. II, 1978.

33. L. I. Maissel and R. Glang, *Handbook of Thin Film Technology*, McGraw-Hill, New York, p. 158, 1970.

34. Gmelin, *Handuch der anorganischen Chemie, Hafnium und Bor, Hauptband*, VCH, Weinbeim, vol. 43, pp. 54, 1951.

35. D. W. Richardson, *Modern Ceramic Engineering*, Marcel Dekker, 2nd Eds., Revised and Expanded, New York, 1992.

36. K. Constant, R. Kieffer and P. Ettmayer, "On the Pseudo-ternary System HfO-HfN-HfC," *Monatsh. Chem.,* vol. 106, pp973-81, 1975.

37. P. G. Cotter and J. A. Kohn, "Industrial diamond substitutes I, physical and X-ray study of hafnium carbide," *J. Am. Ceram. Soc.,* vol. 37, pp. 415-20, 1954.

38. Li- Jian Meng, A. Azevedo and M.. P. dos Santos, "Deposition and properties of titanium nitride films produced by dc reactive magnetron sputtering," *Elsevier Science* , vol. 46(3), pp. 233-239, 1995.

39. B. O. Johansson, J.-E. Sundgren, and U. Helmersson, "Reactively magnetron sputtered Hf-N films. II. Hardness and electrical resistivity," *J. Appl. Phys.,* vol. 58(8), pp. 3112-17, Oct. 1985.

40. O. H. Gokce and N. M. Ravindra, "Applications of RTP in metallization for silicon device technology," *The minerals, Metals & Materials Society*, pp. 37-41, 1996.